

## Photodegradation of phenazopyridine in an aqueous solution by CdS-WO<sub>3</sub> nanocomposite

Farideh Yousefi<sup>a,b</sup>, Alireza Nezamzadeh-Ejchieh<sup>a,b,c,\*</sup>

<sup>a</sup>Department of Chemistry, Shahreza Branch, Islamic Azad University, P.O. Box 311-86145, Shahreza, Isfahan, Iran, emails: arnezamzadeh@iaush.ac.ir (A. Nezamzadeh-Ejchieh), yousefi.f94@gmail.com (F. Yousefi)

<sup>b</sup>Young Researchers and Elite Club, Shahreza Branch, Islamic Azad University, Shahreza, Iran

<sup>c</sup>Razi Chemistry Research Center (RCRC), Shahreza Branch, Islamic Azad University, Isfahan, Iran, Tel. +98 31-53292500

Received 15 May 2019; Accepted 20 November 2019

### ABSTRACT

The as-synthesized CdS-WO<sub>3</sub> nanocomposite and its individual components were characterized by X-ray diffraction, scanning electron microscope, diffuse reflectance spectroscopy, Fourier transformation infra-red spectroscopy and photoluminescence (PL) spectroscopy. The composite was then used in photodegradation of phenazopyridine aqueous solution and it showed a synergistic photocatalytic activity with respect to the individual CdS and WO<sub>3</sub> semiconductors. The composite showed also a lower PL intensity than the single semiconductors. Optimal conditions in photodegradation experiments were C<sub>PhP</sub>: 10 mg L<sup>-1</sup>, pH 4, irradiation time: 45 min and 0.9 g L<sup>-1</sup> of the CdS-WO<sub>3</sub> catalyst when the moles of WO<sub>3</sub> were twice greater than CdS in the composite. The kinetics of the photodegradation process obeyed the Hinshelwood equation and a rate constant of 6.96 × 10<sup>-3</sup> min<sup>-1</sup> with a half-life time of 99.6 min was obtained by UV-Vis spectroscopy. Also, the mineralization extent of the PhP molecules was followed by the COD technique and a rate constant of 0.052 min<sup>-1</sup> with a t<sub>1/2</sub> of 13 min was obtained. HPLC analysis of the PhP solution showed that about 90% of PhP molecules were degraded for 45 min.

**Keywords:** Phenazopyridine; Pseudo-first order kinetic; Heterogeneous photodegradation; Antibiotics; CdS-WO<sub>3</sub> composite

### 1. Introduction

Visible-light photocatalysis based on the semiconducting based photocatalysts has been widely applied for environmental remediation by the degradation of various organic/inorganic/pharmaceutical pollutants. Using visible (solar) light for the excitation of the subjected semiconductor, drastically decreased the cost of the process [1–3]. In this heterogeneous process, the photo-induced electron-hole (e<sup>-</sup>/h<sup>+</sup>) pairs could produce in the conduction (C<sub>b</sub>) and the valence (V<sub>b</sub>) bands of the irradiated semiconductor, respectively. The e<sup>-</sup>/h<sup>+</sup> pairs could, respectively, react with dissolved oxygen and water molecules (or OH anions) to produce superoxide and

hydroxyl radicals. Hence, in a typical semiconducting based photocatalysis, there are four reactive species including e<sup>-</sup>/h<sup>+</sup> pairs, superoxide and hydroxyl radicals that can efficiently attack the investigated pollutant molecules and break them into the smaller fragments and finally mineralize them into carbon dioxide and water molecules, etc. [4–10].

WO<sub>3</sub> is well known as a nontoxic visible-light-driven photocatalyst with a narrow band gap of 2.5–2.8 eV and it has a high oxidation potential of photo-generated holes. The C<sub>b</sub> position of WO<sub>3</sub> has a standard potential in the range of 0–0.5 V (vs. NHE). Comparison of its C<sub>b</sub> position with the E<sup>o</sup> values of –0.33 and 0.05 V for (O<sub>2</sub>/<sup>•</sup>O<sub>2</sub><sup>-</sup>) and (O<sub>2</sub>/HO<sub>2</sub><sup>•</sup>) redox systems confirms that it cannot produce superoxide

\* Corresponding author.

or HO<sub>2</sub> radical. Hence, the photogenerated electrons have a high potential to re-combine with the photogenerated holes. Hence, finding a novel strategy for the fast separation of the photo-induced e<sup>-</sup>/h<sup>+</sup> pairs in the excited WO<sub>3</sub> semiconductor has utmost importance in environmental remediation processes. Generally, for the fast separation of e<sup>-</sup>/h<sup>+</sup> pairs in semiconducting based photocatalysis, different strategies have been used so far by researchers. The most famous of these strategies are doping of a suitable species into the used semiconductor, the coupling of two or more semiconductors, decreasing the path length for the photogenerated e<sup>-</sup>/h<sup>+</sup> pairs to reach them rapidly to the surface of the semiconductor by using nanoparticles, etc. [11–20].

In the present work, both coupling and using of nano-dimension of the semiconductors strategies were used to enhance the photocatalytic activity of WO<sub>3</sub>. For this goal, the p-type semiconductor WO<sub>3</sub> nanoparticles (NPs) were synthesized and coupled mechanically with the as-synthesized n-type CdS NPs. The resulted WO<sub>3</sub>-CdS nanocomposite was then used in photocatalytic degradation of phenazopyridine (PhP) in aqueous solution under visible light irradiation. Phenazopyridine is not an antibiotic and is not recommended for the cure of infection itself. It is a local anesthetic and it is commonly used to relieve symptoms caused by irritation of the urinary tract such as pain, burning, and the feeling of needing to urinate urgently or frequently. It is a dye that acts as a painkiller to soothe the lining of the urinary tract. It has some problems such as toxicity (primarily blood disorders) and potential carcinogenicity that limited its applications. Some side effects of this drugs are pale skin, fever, confusion or weakness, jaundice (yellowing of your skin or eyes), swelling, weight gain, feeling short of breath; blue or purple coloring in our skin, etc.. Hence, we subjected it as the pollutant in the present work that may pollute water sources due to its wide using.

## 2. Experimental

### 2.1. Materials and synthesize procedures

All analytical grade chemicals including CH<sub>3</sub>OH, Cd(NO<sub>3</sub>)<sub>2</sub>·4H<sub>2</sub>O, Na<sub>2</sub>S, ammonium tungstate hydrate (H<sub>42</sub>N<sub>10</sub>O<sub>42</sub>W<sub>12</sub>xH<sub>2</sub>O) and nitric acid as the starting material were prepared from Merck or Sigma-Aldrich Co., (Normal Labo Agency, Isfahan, Iran). Distilled water was used throughout the work. Phenazopyridine (C<sub>11</sub>H<sub>11</sub>N<sub>5</sub>, MW: 213.24) pharmaceutical tablet (100 mg, Shahr-dari Co., Iran) was prepared from local drugstores. Each tablet had 175 mg in weight. For preparing a 100 mg/L of the solution, a PhP tablet was thoroughly hand mixed in an agate mortar to obtain a homogeneous powder. Aliquot 17.5 mg of the powder was dissolved in water and filtered in a 100-mL volumetric flask to remove probable undissolved materials. The resulted solution was diluted to the mark. Diluter solutions were prepared by using the serial dilution method.

For the synthesis of CdS NPs, 100 mL 0.1 M sodium hydroxide aqueous solution and 50 mL CH<sub>3</sub>OH were added dropwise to a 100 mL 0.085 M Cd(NO<sub>3</sub>)<sub>2</sub>·4H<sub>2</sub>O aqueous solution under vigorous stirring (1,200 rpm) for 30 min. Then, 100 mL 0.1 M Na<sub>2</sub>S aqueous solution was added dropwise under 6 h of vigorous stirring. The stirring step was then

continued for an additional 5 h. The resulted CdS NPs were separated by centrifugation (>13,000 rpm) from the green-yellow suspension [21].

To synthesize WO<sub>3</sub> NPs, 45 mL of concentrated nitric acid was added dropwise to 67 mL aqueous solution containing 1.07 mmole of ammonium tungstate hydrate at 80°C. The mixed solution was kept at 80°C for 70 min under a controlled continuous stirring at 800 rpm. Finally, the suspension kept constant for 1 d at room temperature to complete the precipitation. The precipitate was separated by centrifugation at >13,000 rpm and the supernatant was used again for repeating precipitation. The aqueous solution was decanted and distilled water was added with continuous stirring, and then, the sedimentation process was repeated. Finally, the resulted precipitate was dried at 80°C and then calcined at 400°C for 70 min in order to form WO<sub>3</sub> NPs [22].

The following procedure was used for preparing WO<sub>3</sub>-CdS nanocomposite. Adequate amount of each semiconductor (depending on the desired mole ratio for each semiconductor in the resulted composite) was added into an agate mortar and hand-mixed thoroughly for 10 min. After this period, a homogenous powder was obtained.

### 2.2. Characterization

The surface morphology of the as-synthesized composite was studied by scanning electron microscope (SEM; TESCAN CO., Czech Republic). Phase identification of the as-synthesized catalysts was studied by X-ray diffraction (XRD; XPert PRO, with Ni-filtered and Cu-Kα radiation at 1.5406 Å, V: 40 kV, i: 30 mA; Netherlands). The optical properties of the samples were studied by a UV-Vis spectrophotometer equipped with an optics integrating sphere and a diffuse reflectance accessory (JASCOV670, by using BasO<sub>4</sub> as reference. A pH meter (Jenway model 3505, UK) was used to record solutions' pH. A centrifuge (Sigma-Aldrich, 2-16P, Germany) instrument was used for the separation of nanoparticles from the suspensions. A photoluminescence (PL) spectrophotometer (PerkinElmer S45, UK) was used for recording PL spectra. An HPLC chromatogram (Agilent 1200, C<sub>18</sub> reversed-phase, 25 cm in length, 4.6 mm i<sub>d</sub>, particle size column: 5 μm, detector: UV/Vis, UV-A, USA) was used to record the chromatograms.

### 2.3. Photodegradation experiments

In a typical photo-degradation experiment, a suspension of 0.9 g/L of the CdS-WO<sub>3</sub> composite in 10 mg/L PhP solution at pH 4 was subjected to the irradiation process. The radiation source was a 100 W tungsten lamp (Osram electric Co., Iran) which was positioned 15 cm above the reaction cell. The reaction cell was a common 25 mL beaker. The suspension was stirred continuously on a magnetic stirrer (200 rpm) to achieve a homogeneous suspension for increasing the repeatability of the experiments. At definite time intervals, an aliquot of sample was withdrawn and centrifuged (at 13,000 rpm, g: 15,493). The absorbance of the supernatant (A) was recorded at a maximum absorption wavelength of PhP (426 nm) and comprised with the absorbance of blank PhP solution (A<sub>0</sub>) at the same concentration. Because the absorbance corresponds to concentration (C<sub>0</sub> and C, the initial and

final PhP concentrations, respectively) based on the Beer-Lambert law, the ratio of  $A/A_0$  was considered as a measure of  $C/C_0$ . The  $C/C_0$  value, in turn, counted as a measure of the degraded PhP molecules during the photodegradation process. When degradation extent (DE) of PhP was followed, we used the following equation [23].

$$DE\% = \left[ \left( \frac{1-A}{A_0} \right) \right] \times 100 \quad (1)$$

#### 2.4. Formula and equations

For estimation of the crystallite size of the composite ( $d$ ), the following Scherrer equation was used. In this equation, term  $\beta$  is excess of width line of the diffraction peak (in radian), term  $\theta$  is the Bragg's angle (in degree) and  $\lambda$  is the wavelength of X-ray photons [24,25].

$$d = \frac{0.9 \lambda}{\beta \cos\theta} \quad (2)$$

To calculate the band gap energy ( $E_g$ ) of the used samples by using the absorption edge wavelengths ( $\lambda_{AE}$ ), the following formula was used [26–28].

$$Eg(eV) = \frac{1240}{\lambda_{AE}(nm)} \quad (3)$$

To calculate the rate constant ( $k$ ) of the pseudo-first-order reaction, the following Hinshelwood equation was used. Also, for the estimation of  $t_{1/2}$  of the process, the  $t_{1/2} = 0.693/k$  formula was used [29,30]. In the Hinshelwood equation,  $C_0$  and  $C$  show the initial and final concentrations of the solution.

$$\ln\left(\frac{C}{C_0}\right) = -kt \quad (4)$$

To evaluate the precision of the reusing method the following statistical 'g-test' formula was used in which  $s_i^2$  is the variance of each class of determinations [31].

$$g = \frac{\text{largest } s^2}{s_1^2 + s_2^2 + s_3^2 + s_4^2} \quad (5)$$

### 3. Results and discussion

#### 3.1. Characterizations

##### 3.1.1. XRD patterns

Fig. 1 shows the XRD pattern of the CdS-WO<sub>3</sub> composite which some important peaks are assigned to the corresponding  $hkl$  planes. It was reported that the hexagonal crystallite phase of CdS includes typical diffraction peaks at  $2\theta$  positions of 24.96°, 26.63°, 28.31°, 36.69°, 43.71°, 47.86°, 51.85°, 52.73°, 55.16°, 58.18°, 62.73°, 66.61°, 69.01°. These reflection peaks correspond to  $hkl$  planes of (100), (002), (101), (102), (110), (103), (112), (201), (004), (202), (104), (203), (210), respectively,

according to JCPDS card No. 41–1049 and 80–0006 [32,33]. Based on literature [34], the hexagonal phase of WO<sub>3</sub> includes typical diffraction peaks positioned at  $2\theta$  values of 14.09°, 22.90°, 24.36°, 26.97°, 28.30° and 36.64° corresponding to  $hkl$  planes of (100), (001), (110), (101), (200) and (201) planes, respectively (JCPDS file no. 351001). The recorded pattern of the composite in this work includes the aforementioned diffraction peaks and well agreement is present. Accordingly, the observed peaks of the composite are assigned to their corresponding  $hkl$  planes as shown in Fig. 1.

By using the Scherrer equation (Eq. (2)), the average crystallite size of the composite was estimated at about  $22.4 \pm 10.3$  nm. All data used for this calculation are summarized in SDT1 (see supplementary data).

##### 3.1.2. Optical properties of the CdS-WO<sub>3</sub> composite

The electronic excitation of a semiconductor determines its band gap energy and is an important parameter in semiconducting based photocatalysis because a narrower band gap generates more photogenerated  $e^-/h^+$  pairs in the irradiated semiconductor. One way to achieve a narrower band gap is the coupling of two or more semiconductors that hybrids the energy levels and may cause a narrower band gap. To estimate the band gap energy of the individual CdS and WO<sub>3</sub> semiconductors and their composite, and also to study of change in the band gap energy during the coupling process, UV-Vis diffuse reflectance spectra of the samples were recorded. Typical absorption plots are shown in Fig. 2a. In these spectra, absorption edge wavelength of each sample was estimated which corresponds to electronic excitation of the samples. The extrapolated absorption edge wavelengths ( $\lambda_{AE}$ ) were used to estimate the band gap energy ( $E_g$ ) by using Eq. (3). The results are summarized in the inset of Fig. 2a. As shown, the composite showed a small red shift in the band gap with respect to WO<sub>3</sub> NPs while it showed a small blue shift with respect to CdS NPs. However, coupling of these semiconductors improved the optical properties of WO<sub>3</sub> NPs [35,36].

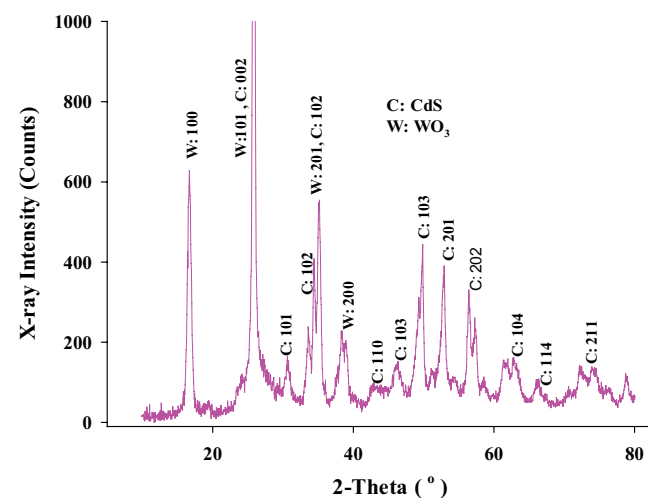


Fig. 1. Typical XRD pattern of the as-synthesized CdS-WO<sub>3</sub> nano-composite (mole ratio of 1:2).

As we know,  $e^-/h^+$  recombination in a photo-excited compound (such as a semiconductor) is a positive phenomenon in PL process while it is a negative phenomenon in a photodegradation processes [37,38]. Hence, to measure the  $e^-/h^+$  recombination extent in the individual CdS and  $WO_3$

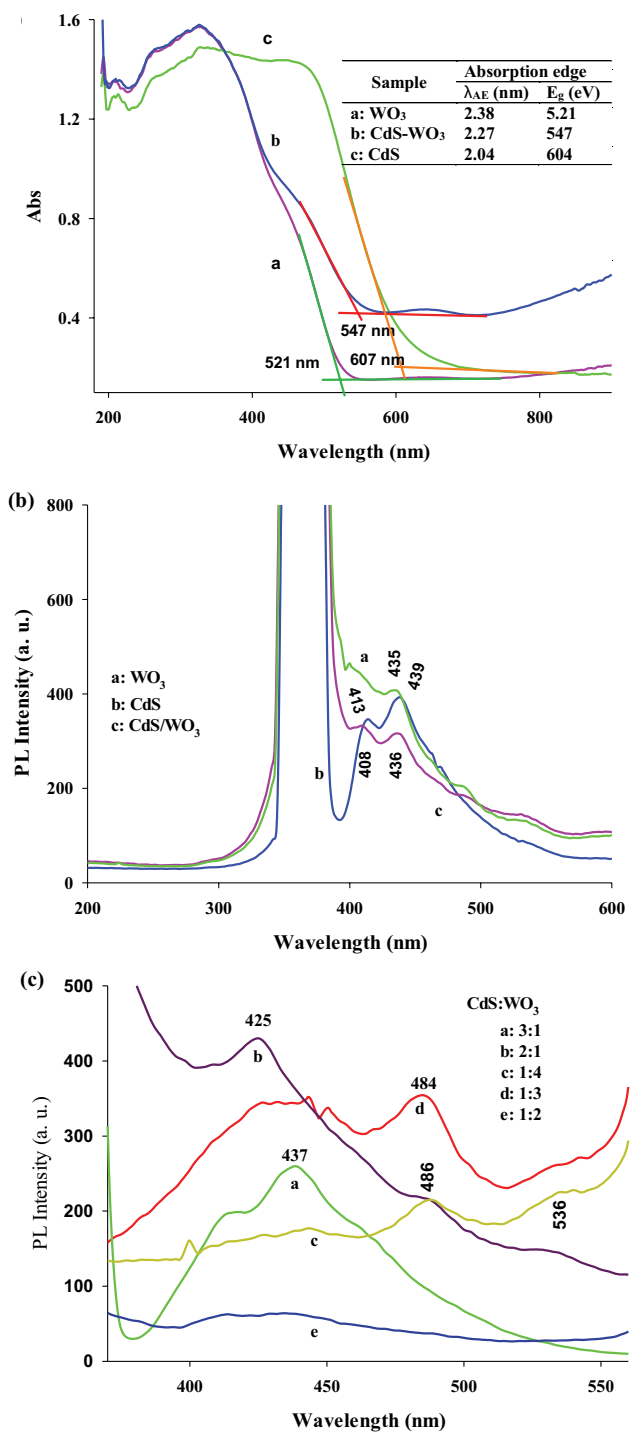


Fig. 2. (a) Typical absorption spectra of the samples obtained in DRS study; (b) photoluminescence (PL) spectra of the samples; (c) change in PL intensity of the nanocomposite as a function of mole ratio of the ingredients (PL conditions: 80 mg/L in acetone;  $\lambda_{ex}$ : 360 nm).

NPs and the resulted nano-composite, PL spectra of the samples were recorded in acetone solvent and shown in Fig. 2b. As shown, the PL intensity of the composite (for the peaks centered at 408 and 436 nm) was decreased with respect to the individual systems. This confirms a slower  $e^-/h^+$  recombination process is carried out in the composite that can cause a better photodegradation efficiency for it. This speculation will discuss in the photodegradation section.

Fig. 2c shows that the PL intensity of the CdS- $WO_3$  composite depends on the mole ratio of the coupled semiconductors. On the other hand, a change in the mole ratio of CdS and  $WO_3$  in the resulted composites can change the  $e^-/h^+$  recombination rate. As shown, the lowest PL intensity was obtained for the composite with the CdS/ $WO_3$  mole ratio of 1:2. As we will see in the photodegradation section, this composite shows the best photodegradation efficiency. In all PL spectra, the high intense peak at 360 nm shows the light scattered by the nano-samples.

### 3.1.3. Investigation of surface charge of the composite

To evaluate the surface charge of the samples, the initial pH ( $pH_i$ ) of suspensions containing 0.09 g of each catalyst in 5 mL 0.1 M NaCl was adjusted between 2 and 10 and shaken for 24 h. The final pH ( $pH_f$ ) was recorded and drawn against the  $pH_i$ . The crossing point of the curve with bisector ( $pH_i$  vs.  $pH_f$ ) gave the pH of point of zero charge ( $pH_{pzc}$ ) of the catalyst (Fig. 3) [39–41]. As shown below, the  $pH_{pzc}$  value, the initial pHs were increased showing that the catalyst surfaces have a basic property and hence adsorb protons of the adjacent solution. Hence, the surface of the catalysts acquires a net positive charge and the pH of the solution was increased. At pHs above  $pH_{pzc}$  the initial pHs were decreased. This confirms an acidic property of the catalyst surface that resulted to adsorb hydroxyl anions from the adjacent solution. Hence, the surface of the catalysts gave a net negative charge and the pH of the solution was decreased. At  $pH_{pzc}$  the basic property of the catalyst surface begun to change to an acidic property. At this point, the charge of the catalyst surface was neutralized by the adjacent solution. The  $pH_{pzc}$  of CdS,  $WO_3$  NPs, and the CdS- $WO_3$  composite was

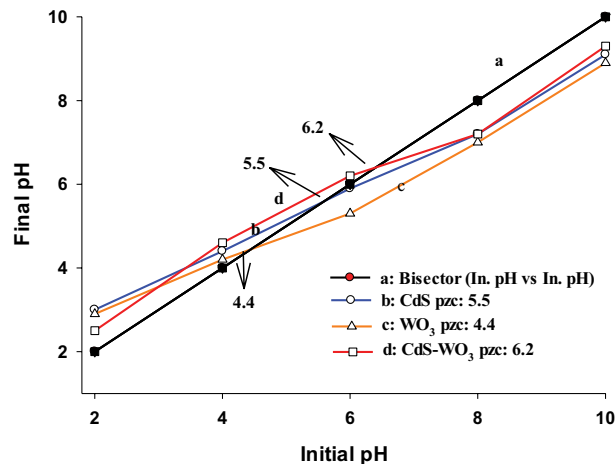


Fig. 3. Plots of determination of  $pH_{pzc}$  of the catalysts.

estimated at about 5.5, 4.4 and 6.2, respectively. A discussion on  $\text{pH}_{\text{pzc}}$  with more details is present in our previous work [42].

### 3.1.4. SEM studies

Fig. 4 shows some SEM images of the CdS-WO<sub>3</sub> composite with a mole ratio of 1:2 for CdS:WO<sub>3</sub>. The images show that some spherical NPs are dispersed on the nano-flakes. The nano-flakes belong to WO<sub>3</sub> species. These smooth nano-flakes of WO<sub>3</sub> are randomly distributed in different directions and the CdS NPs are dispersed on them homogeneously. The images confirm the formation of nano-dimension for the composite.

## 3.2. Photodegradation results

### 3.2.1. Photocatalytic activity

Fig. 5a shows a decrease in UV-Vis absorption spectra of PhP solutions during different initial experiments. This decrease shows the removal of PhP molecules during the mentioned processes. The corresponding  $C/C_0$  values as a measure of the removed PhP are shown in the inset of Fig. 5a. Accordingly, 7% and 9.2% of the initial PhP molecules are removed by direct photolysis and surface adsorption for 20 min, respectively. The role of surface adsorption on PhP removal was also followed at contacting times of 30, 45 and 60 min. The results showed that about 10.8%, 11.5% and 12.0% of the molecules were removed at the mentioned

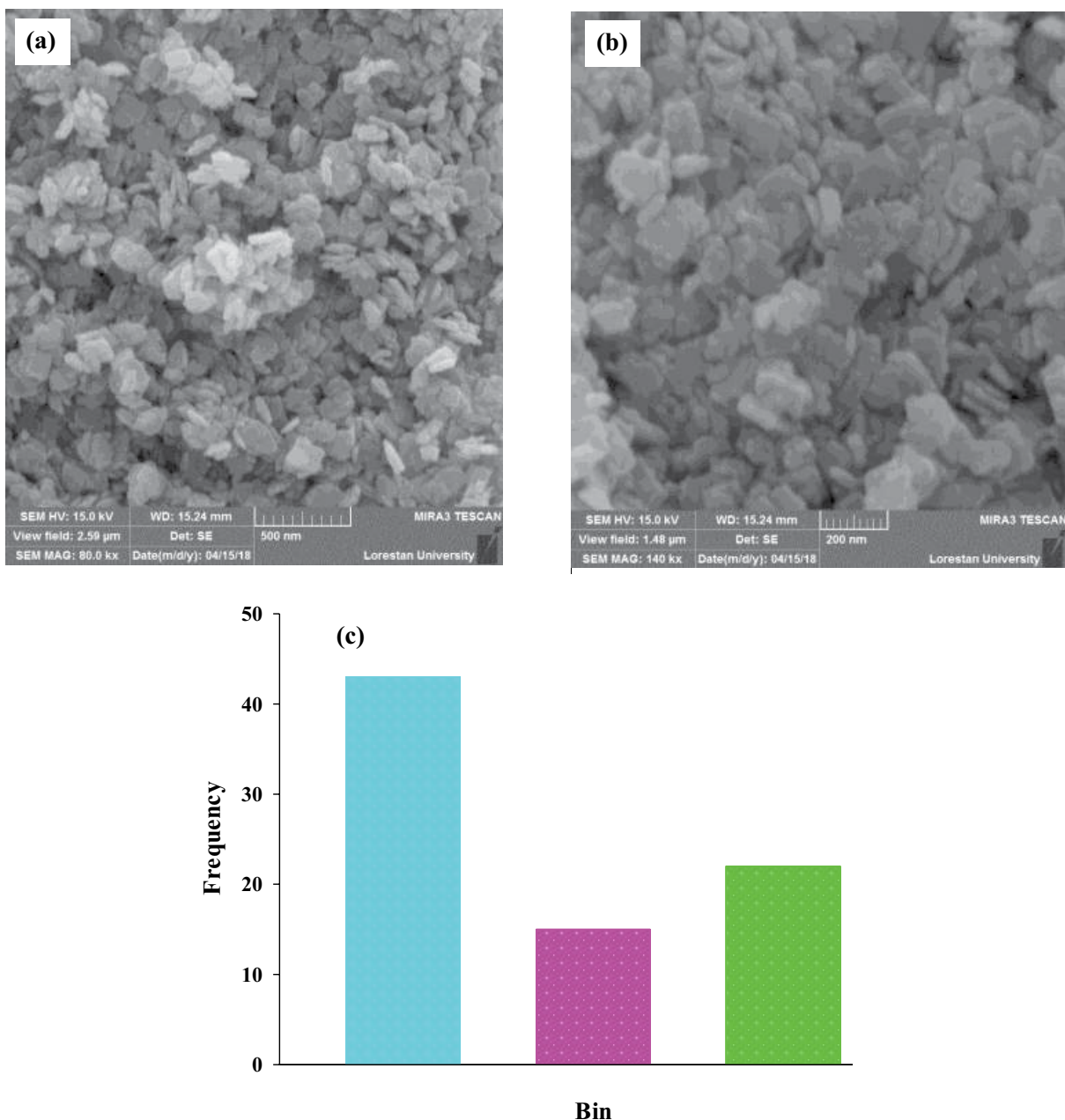


Fig. 4. SEM images of the CdS-WO<sub>3</sub> composite (a, b); Particle size distribution obtained by applying image-j software on image B (c)

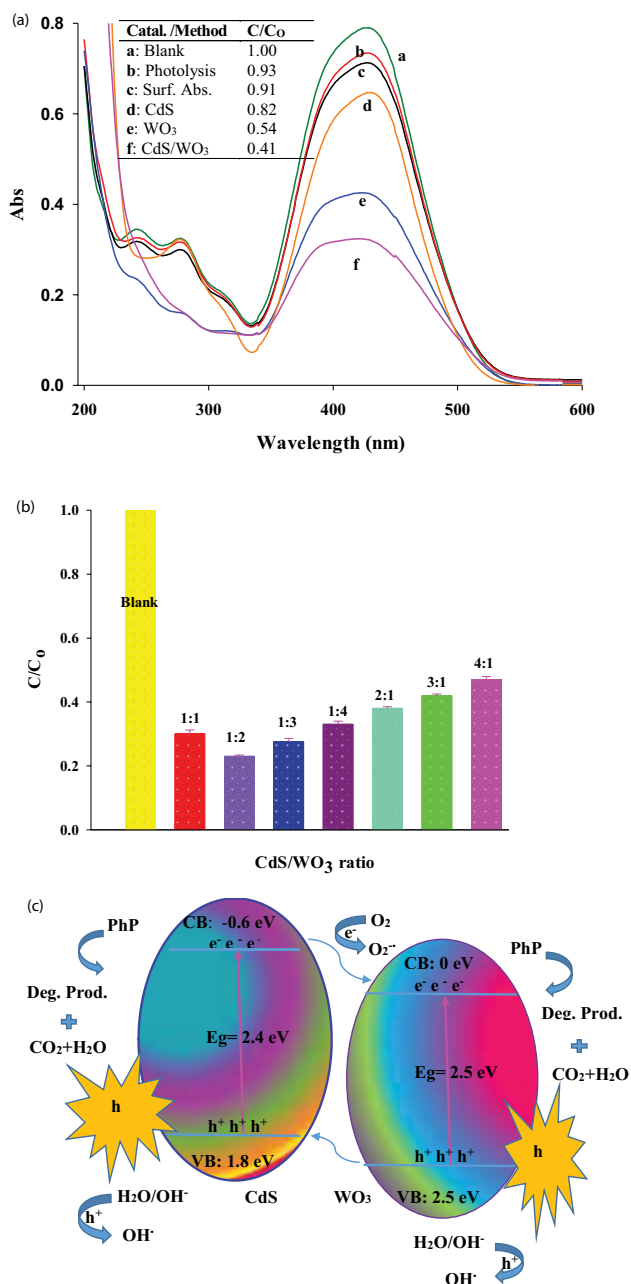


Fig. 5. Effects of different removal processes on PhP removal (catalysts dose: 0.3 g L<sup>-1</sup>, C<sub>PhP</sub>: 10 mg L<sup>-1</sup>, time: 20 min, initial pH: 4); (b) Effects of the mole ratio of the CdS-WO<sub>3</sub> in photodegradation of PhP at the aforementioned conditions (c) The schematic energy diagram for the charge carriers' transfer in the composite.

times, respectively. Because of no significant difference in the removal by surface adsorption at longer times, before all photodegradation experiments, the suspensions were shaken for 20 min at dark to reach equilibrium adsorption/desorption process. As the results show, the photodegradation method is the most efficient method to remove PhP molecules from the solution with a boosted activity of the composite with respect to the individual WO<sub>3</sub> and CdS systems. During 20 min photodegradation of PhP solution

about 18%, 46% and 60% of the molecules were degraded by CdS, WO<sub>3</sub> and CdS-WO<sub>3</sub> composite (with a mole ratio of 1:1), respectively. This boosted activity of the composite relates to the better charge carriers' transfer in the composite [43,44].

To achieve a better-boosted activity of the composite, the mole ratio of its ingredients was changed and the photocatalytic activity of the resulted composites was followed. The results are shown in Fig. 5b which shows the photocatalytic activity of the composite depends on the mole ratio of its ingredients [45].

Typical schematic energy diagram of charge carriers' transfer in the photo-excited composite is shown in Fig. 5c. Both semiconductors of the composite have band gap energy in the visible light region and hence they can excite by the arrived visible photons. The photogenerated electrons in the conduction band (C<sub>b</sub>) of CdS have a standard E<sup>o</sup> value of -0.6 V (vs. NHE) that is more negative than that of the WO<sub>3</sub>-C<sub>b</sub> level (0 V). This favors an internal oxidation-reduction process and hence the electron in the CdS-C<sub>b</sub> immigrates to the WO<sub>3</sub>-C<sub>b</sub> level. In the opposite way, the E<sup>o</sup> value of the valence band (V<sub>b</sub>) of WO<sub>3</sub> is about 2.5 V which is more positive than that of the CdS-V<sub>b</sub> (1.86 V). This favors the hole transfer from WO<sub>3</sub>-V<sub>b</sub> to the CdS-V<sub>b</sub> level. In addition, the WO<sub>3</sub>-C<sub>b</sub> level has more negative E<sup>o</sup> value with respect to that of the CdS-V<sub>b</sub> level. Hence, the photogenerated electrons in the WO<sub>3</sub>-C<sub>b</sub> can immigrate to the CdS-V<sub>b</sub> level. Hence, all the aforementioned pathways favor charge carriers' separation in the composite that diminishes the rate of e<sup>-</sup>/h<sup>+</sup> recombination process. This is the pivotal factor for the boosted photocatalytic activity of the composite.

When moles of WO<sub>3</sub> are twice greater than CdS, the best matching is present to achieve the best-mentioned charge separation. When moles of WO<sub>3</sub> or CdS were increased from this optimum value, the photocatalytic activity of the resulted composites was decreased.

### 3.2.2. Kinetics and mineralization of the process

As we know, when the initial pollutant and its degradation intermediates absorb the arrived photons, the degradation rate can be evaluated by the following Grotthuss-Draper law. This law relates to the Beer-Lambert law [46,47] at which the initial and final (at time t) concentrations of pollutants are C<sub>0</sub> and C, the rate constant is k<sub>1</sub> and the absorption coefficients of the pollutant and the products are k<sub>2</sub> and k<sub>3</sub>, respectively.

$$-\frac{dC}{dt} = k_1 \left( 1 - \exp \left[ - \left( k_2 C + k_3 (C_0 - C) \right) \right] \right) \left[ \frac{k_2 C}{(k_2 C + k_3 (C_0 - C))} \right] \quad (6)$$

When the photodegradation products do not absorb the arrived photons, k<sub>3</sub> is about zero. In the case of high concentrated reactant, the process obeys zero-order kinetics. When k<sub>3</sub> ~ k<sub>2</sub>, it means that the photodegradation intermediates have the same spectrum with the reactant, and hence a pseudo-first-order reaction rate (not a first-order one) must be achieved and hence Eq. (6) can be simplified as Eq. (7), at which k is the pseudo-first-order reaction rate constant [46,47].

$$-\frac{dC}{dt} = k_1(1 - \exp[-k_2 C_0]) \left(\frac{C}{C_0}\right) = kC \quad (7)$$

Eq. (8) shows the integrated form of Eq. (7) that is similar to the Hinshelwood pseudo-first-order reaction rate constant [29,30].

$$\ln\left(\frac{C}{C_0}\right) = -Kt \quad (\text{or } C_t = C_0 e^{-kt}) \quad (8)$$

Hence, the kinetics of PhP photodegradation by the as-synthesized CdS-WO<sub>3</sub> composite was followed. A decrease in  $C/C_0$  values during the photodegradation process is shown in Fig. 6a. The resulted plot of  $\ln(C/C_0)$  vs. irradiation time is shown in the inset. The slope of the curve is  $6.96 \times 10^{-3} \text{ min}^{-1}$  that shows the pseudo-first-order reaction rate constant of the process. Accordingly, the  $t_{1/2}$  value was estimated at about 99.6 min. A discussion on the kinetics of the photodegradation process with more details is present in our previous work [48].

As we know, the pollution extent of an aquatic sample can be estimated from its chemical oxygen demand (COD) value and a lower pollution results in a lower COD value [49,50]. Accordingly, when a typical pollutant mineralizes to carbon dioxide, water molecules, etc., the COD value of its aqueous solution tends to decrease. Thus, the COD value of such a solution estimates its mineralization extent. PhP solutions, before and after photodegradation experiments, were subjected to COD analysis and the results are shown in Fig. 6b. Based on the inset of this figure, a rate constant of  $0.052 \text{ min}^{-1}$  (and  $t_{1/2} = 13.3 \text{ min}$ ) was obtained for mineralizing of PhP at the applied conditions. This value is 7.5 times greater than that of degradation rate constant obtained by UV-Vis spectroscopy ( $6.96 \times 10^{-3} \text{ min}^{-1}$ ). This comparison confirms that initial PhP molecules may resist degradation process during initial times and when it was degraded to smaller fragments, these intermediates rapidly mineralized to CO<sub>2</sub>, H<sub>2</sub>O, etc.

### 3.2.3. HPLC and reusability measurements

HPLC chromatograms of PhP solutions before and after 45 min photodegradation process are shown in Fig. 7a. As shown, the main peak of the solution at a retention time of 27.25 min was drastically decreased during the photodegradation process. This corresponds to a degradation of 90% of the molecules for 45 min. Such a solution had a degradation extent of 86% obtained by UV-Vis spectroscopy. These values are close together because the HPLC detector was a UV detector. A new peak was detected at a retention time of 28.32 min that accompanied with a broad peak ranged from 20 min to about 29 min, confirming the formation of new smaller degradation intermediates. No attempt was done to detect these intermediates. Mobile phase contained a solvent programming of 15%–25% 'A' and 85%–75% 'B' component (A: methanol and B: phosphate buffer at pH 6.5 [10 mM]) for 15 min, then to 80% A, and 20% B over a 10 min period by using a linear gradient program [51].

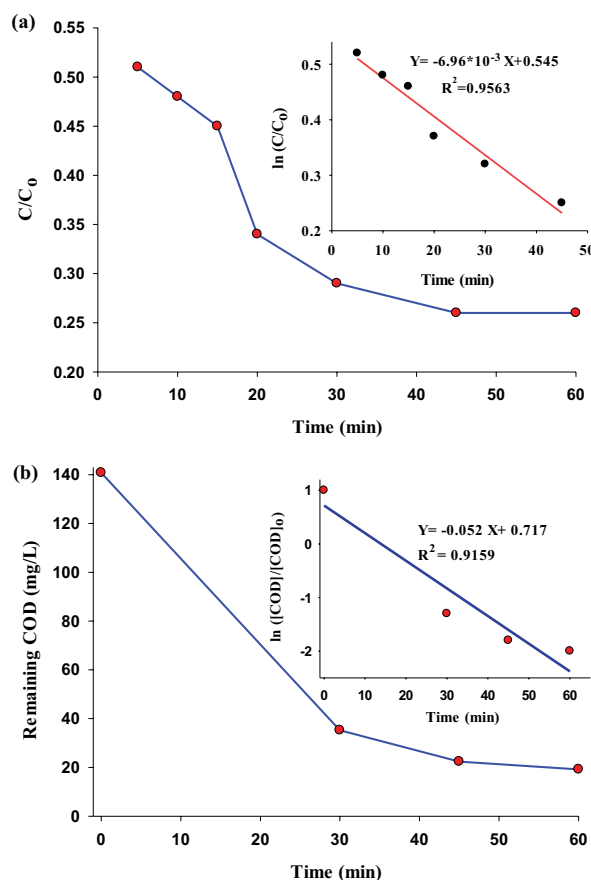


Fig. 6. (a) Change in  $C/C_0$  values during irradiation time in the photodegradation of PhP; Inset: Typical  $\ln(C/C_0)$ –time plot for photodegradation of PhP. (b) Change in COD values of PhP solution (Inset: Typical plot for the study of mineralization rate of PhP). Conditions in both cases: dose of the catalyst:  $0.9 \text{ g L}^{-1}$ ,  $C_{\text{PhP}} = 10 \text{ mg L}^{-1}$ , pH 4).

The reusability of the composite catalyst was evaluated in PhP photodegradation. For this goal, the catalyst was re-used in three successive runs and after each run, the catalyst was dried at  $80^\circ\text{C}$  for 15 min. The results are summarized in Fig. 7b. In this study, the kinetics of the process in each run was evaluated. All data in each run were averaged based on triplicate measurements. The average rate constants of  $3.89 (\pm 0.57) \times 10^{-2}$ ,  $3.46 (\pm 0.54) \times 10^{-2}$ ,  $3.97 (\pm 0.71) \times 10^{-2}$  were obtained for runs 1–3, respectively. These values were statistically evaluated by the  $g$ -test (Eq. (5)). The calculated  $g$  value is 0.4466 which is smaller than its critical  $g$  value at 95% confidence interval,  $g_{0.05,3,3} = 0.9423$  (3 class ( $k$ ), three replicates ( $n$ ) in each class,  $g_{0.05,n,k}$ ). This confirms that there is no difference between the averaged rate constants of 3 aforementioned runs and the appeared differences are due to random errors. This comparison confirms that the catalyst can retain its initial activity after three successive runs and no significant decrease in its activity can occur with 95% certainty [52].

### 3.2.4. FTIR study of PhP sample

Fourier transformation infra-red (FTIR) spectra of PhP solutions before (blank) and after photodegradation process

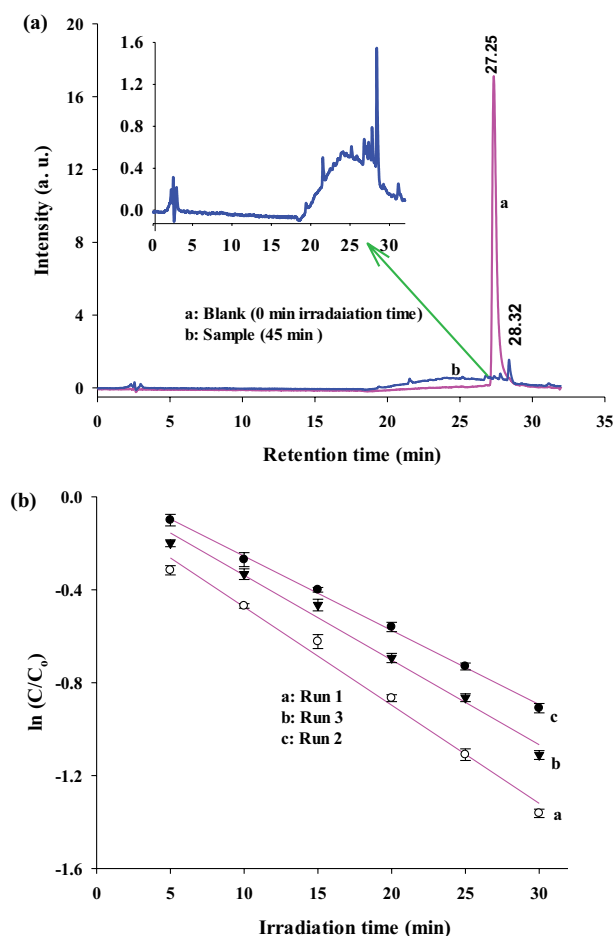


Fig. 7. (a) Change in HPLC chromatograms of PhP solution before (a) and after photodegradation process (b); (b) Results of reusing experiments. Conditions in both cases: 0.9 g L<sup>-1</sup> of the composite catalyst, C<sub>PhP</sub> = 10 mg L<sup>-1</sup>, pH 4 at irradiation time of 45 min.

(sample) (photodegradation conditions: 0.9 g/L of the catalyst, 10 mg/L of PhP, pH 4, 45 min) were recorded and shown in Fig. 8. To separate PhP from solution, a liquid-liquid extraction method was used. For this goal, 1 mL of 1 M NaOH was added to the solution and then 2.5 mL ethyl acetate-diethyl ether (1:1) was added and the mixture was vortexed for 5 min. Finally, the solution was centrifuged for 10 min (4,000 rpm) and the upper organic layer was transferred to a clean tube. The lower aqueous solution was subjected to the extraction process for another time. The organic solution was evaporated under a stream of nitrogen at 40°C [53]. The remained PhP phase was used for recording the FTIR spectra against KBr pellets.

Typical vibration of aromatic and alkenes' C=C can show absorption peaks at 1,400–1,600 cm<sup>-1</sup> and 1,620–1,680 cm<sup>-1</sup>, respectively. Typical bands at 1,463 cm<sup>-1</sup> in the spectrum of blank corresponds to the aromatic C=C while the peaks located at 1,463; 1,554 and 1,653 cm<sup>-1</sup> in sample spectrum correspond to that of alkenes compounds. The N–H vibration mode showed absorption bands at 3,513 and 3,635 cm<sup>-1</sup> in the spectra of PhP samples. After the photodegradation experiment, these peaks overlapped with OH stretching

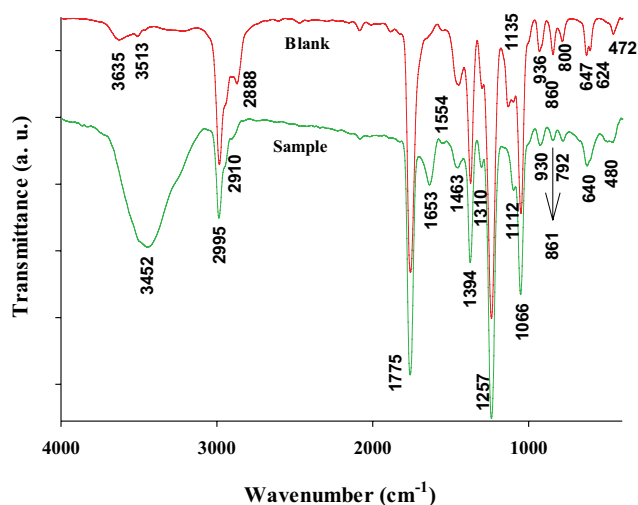


Fig. 8. FTIR spectra of PhP solution before (blank) and after photodegradation process (sample).

mode and created a broad peak at 3,452 cm<sup>-1</sup>. The main change in the spectra is the appearance of the corresponding OH stretching vibration. Typical peaks of carbonyl group located at 1,775 cm<sup>-1</sup> present in both spectra. In spectrum of blank sample, this peak can be related to atmospheric carbon dioxide. In the spectrum of the sample, this peak can also be related to carbonyl compounds formed during the degradation of PhP. In general, the presence of the peaks of OH and C=O functional groups in the spectrum of the sample confirm some acidic and alcoholic compounds formed during the photodegradation process.

#### 4. Conclusion

As-synthesized CdS-WO<sub>3</sub> nano-composite showed a synergistic catalytic effect in photodegradation of PhP aqueous solution with respect to single CdS or WO<sub>3</sub> NPs. This is due to a lower e<sup>-</sup>/h<sup>+</sup> recombination in the composite. The composite showed also a lower PL intensity than WO<sub>3</sub> and CdS alone. This confirmed a lower e<sup>-</sup>/h<sup>+</sup> recombination process occurred in the composite. The mineralization extent of PhP solution was followed by COD analysis. Simultaneously, the degradation of PhP molecules was followed by UV-Vis measurement on similar solutions. The rate constants of 0.052 min<sup>-1</sup> and 6.96 × 10<sup>-3</sup> min<sup>-1</sup> were, respectively, obtained for the mineralization and degradation processes, respectively. On the other hand, mineralization rate of PhP was about 7.5 times faster than its degradation extent. This confirms that initial PhP molecules may resist degradation at initial steps, but the produced intermediates may rapidly mineralize water, carbon dioxide, etc.

#### Acknowledgements

The authors thank Mohammad Alizadeh and Mohammad Hossein Kazemzadeh for performing instrumental analysis of the samples, as experts in the laboratory analysis in Shahreza Branch, Islamic Azad University. The authors also thank from Dr. Farid Naeimi as the university president for supporting of this work.

## References

- [1] A. Nezamzadeh-Ejhih, Z. Banan, Sunlight assisted photodecolorization of crystal violet catalyzed by CdS nanoparticles embedded on zeolite A, *Desalination*, 284 (2012) 157–166.
- [2] D. Zhang, J. Wang, Visible-light-responsive bismuth oxybromide/graphite-like C<sub>3</sub>N<sub>4</sub> hybrid material and its application in photocatalysis via internal electric field, *J. Iranian Chem. Soc.*, 16 (2019) 827–839.
- [3] N. Elmi Fard, R. Fazaeli, Experimental design study of RB 255 photocatalytic degradation under visible light using synthetic Ag/TiO<sub>2</sub> nanoparticles: optimization of experimental conditions, *Iran. J. Catal.*, 8 (2018) 133–141.
- [4] Zh. Wang, H. Zhang, H. Cao, L. Wang, Z. Wan, Y. Hao, X. Wang, Facile preparation of ZnS/CdS core/shell nanotubes and their enhanced photocatalytic performance, *Int. J. Hydrogen Energy*, 42 (2017) 17394–17402.
- [5] M. Zhu, Y. Li, Sh. Tian, Y. Xie, X. Zhao, X. Gong, Deep-red emitting zinc and aluminium co-doped copper indium sulfide quantum dots for luminescent solar concentrators, *J. Colloid Interface Sci.*, 534 (2019) 509–517.
- [6] K. Thirumalaia, M. Shanthi, S. Swaminathan, Natural sunlight active GdVO<sub>4</sub>-ZnO nanomaterials for photo-electrocatalytic and self-cleaning applications, *J. Water Proc. Eng.*, 17 (2017) 149–160.
- [7] S.P. Meshram, P.V. Adhyapak, U.P. Mulik, D.P. Amalnerkar, Facile synthesis of CuO nanomorphs and their morphology dependent sunlight driven photocatalytic properties, *Chem. Eng. J.*, 204–206 (2012) 158–168.
- [8] Ch. EL Bekkali, H. Bouyarmane, S. Laasri, A. Laghzizil, A. Saoiabi, Effects of metal oxide catalysts on the photodegradation of antibiotics effluent, *Iran. J. Catal.*, 8 (2018) 241–247.
- [9] T. Liu, M. Li, X. Bo, M. Zhou, Designing iron carbide embedded isolated boron (B) and nitrogen (N) atoms codoped porous carbon fibers networks with tiny amount of B-N bonds as high efficiency oxygen reduction reaction catalysts, *J. Colloid Interface Sci.*, 533 (2019) 709–722.
- [10] K. Prakash, S. Karuthapandian, S. Senthilkumar, Zeolite nanorods decorated g-C<sub>3</sub>N<sub>4</sub> nanosheets: a novel platform for the photodegradation of hazardous water contaminants, *Mater. Chem. Phys.*, 221 (2019) 34–46.
- [11] N.L. Subbulekshmi, E. Subramanian, Nano CuO immobilized fly ash zeolite Fenton-like catalyst for oxidative degradation of p-nitrophenol and p-nitroaniline, *J. Environ. Chem. Eng.*, 5 (2017) 1360–1371.
- [12] P. Raizada, J. Kumari, P. Shandilya, P. Singh, Kinetics of photocatalytic mineralization of oxytetracycline and ampicillin using activated carbon supported ZnO/ZnWO<sub>4</sub> nanocomposite in simulated wastewater, *Desal. Wat. Treat.*, 79 (2017) 204–213.
- [13] N. Sapawe, A.A. Jalil, S. Triwahyono, One-pot electro-synthesis of ZrO<sub>2</sub>-ZnO/HY nanocomposite for photocatalytic decolorization of various dye-contaminants, *Chem. Eng. J.*, 225 (2013) 254–265.
- [14] N. Masoudipour, M. Sadeghi, F. Mohammadi-Moghadam, Photo-catalytic inactivation of *E. coli* using stabilized Ag/S, N-TiO<sub>2</sub> nanoparticles by fixed bed photo-reactor under visible light and sunlight, *Desal. Wat. Treat.*, 110 (2018) 109–116.
- [15] A. Rostami-Vartooni, A. Moradi-Saadatmand, M. Bagherzadeh, M. Mahdavi, Green synthesis of Ag/Fe<sub>3</sub>O<sub>4</sub>/ZrO<sub>2</sub> nanocomposite using aqueous *Centaurea cyanus* flower extract and its catalytic application for reduction of organic pollutants, *Iran. J. Catal.*, 9 (2019) 27–35.
- [16] A. Nezamzadeh-Ejhih, M. Bahrami, Investigation of the photocatalytic activity of supported ZnO-TiO<sub>2</sub> on clinoptilolite nano-particles towards photodegradation of wastewater-contained phenol, *Desal. Wat. Treat.*, 55 (2015) 1096–1104.
- [17] K. Kanti Bera, R. Majumdar, M. Chakraborty, S. Kumar Bhattacharya, Phase control synthesis of  $\alpha,\beta$  and  $\alpha/\beta$ Bi<sub>2</sub>O<sub>3</sub> hetero-junction with enhanced and synergistic photocatalytic activity on degradation of toxic dye, Rhodamine-B under natural sunlight, *J. Hazard. Mater.*, 352 (2018) 182–191.
- [18] S. Landi Jr, J. Carneiro, S. Ferdov, António M. Fonseca, Isabel C. Neves, M. Ferreira, P. Parpot, Olivia S.G.P. Soares, Manuel F.R. Pereira, Photocatalytic degradation of Rhodamine B dye by cotton textile coated with SiO<sub>2</sub>-TiO<sub>2</sub> and SiO<sub>2</sub>-TiO<sub>2</sub>-HY composites, *J. Photochem. Photobiol., A*, 346 (2017) 60–69.
- [19] B.A. Ünnü, G. Gündüz, M. Dükkancı Heterogeneous Fenton-like oxidation of crystal violet using an iron loaded ZSM-5 zeolite, *Desal. Wat. Treat.*, 57 (2016) 11835–11849.
- [20] H. Che, G. Che, E. Jiang, Ch. Liu, H. Dong, Ch. Li, A novel Z-Scheme CdS/Bi<sub>2</sub>O<sub>3</sub>Cl heterostructure for photocatalytic degradation of antibiotics: mineralization activity, degradation pathways and mechanism insight, *J. Taiwan Inst. Chem. Eng.*, 91 (2018) 224–234.
- [21] N. Qutub, B. Pirzada, Kh. Umar, S. Sabir, Synthesis of CdS nanoparticles using different sulfide ion precursors: formation mechanism and photocatalytic degradation of Acid Blue-29, *J. Environ. Chem. Eng.*, 4 (2016) 808–817.
- [22] A. Martinez-de la Cruz, D. Sanchez Martinez, E. Lopez Cuellar, Synthesis and characterization of WO<sub>3</sub> nanoparticles prepared by the precipitation method: evaluation of photocatalytic activity under vis-irradiation, *Solid State Sci.*, 12 (2010) 88–94.
- [23] L. Daneshvar, A. Nezamzadeh-Ejhih, Photocatalytic activity of ZnO nanoparticles towards tinidazole degradation: experimental design by response surface methodology (RSM), *Desal. Wat. Treat.*, 141 (2019) 364–376.
- [24] Z.-Alsadat Mirian, A. Nezamzadeh-Ejhih, Removal of phenol content of an industrial wastewater via a heterogeneous photodegradation process using supported FeO onto nanoparticles of Iranian clinoptilolite, *Desal. Wat. Treat.*, 57 (2016) 16483–16494.
- [25] S. Dharmraj Khairnar, M. Rajendra Patil, V. Shankar Shrivastava, Hydrothermally synthesized nanocrystalline Nb<sub>2</sub>O<sub>5</sub> and its visible-light photocatalytic activity for the degradation of congo red and methylene blue, *Iran. J. Catal.*, 8 (2018) 143–150.
- [26] M. Karimi-Shamsabadi, M. Behpour, A. Kazemi Babaheidari, Z. Saberi, Efficiently enhancing photocatalytic activity of NiO-ZnO doped onto nanozeoliteX by synergistic effects of p-n heterojunction, supporting and zeolite nanoparticles in photodegradation of Eriochrome Black T and Methyl Orange, *J. Photochem. Photobiol., A*, 346 (2017) 133–143.
- [27] H.R. Pouretedal, M. Fallahgar, F.S. Pourhasan, M. Nasiri, Taguchi optimization of photodegradation of yellow water of trinitrotoluene production catalyzed by nanoparticles TiO<sub>2</sub>/N under visible light, *Iran. J. Catal.*, 7 (2017) 317–326.
- [28] M.H. Habibi, P. Bagheri, Spinel cobalt manganese oxide nanocomposites grown hydrothermally on nanosheets for enhanced photocatalytic mineralization of Acid Black 1 textile dye: XRD, FTIR, FESEM, EDS and TOC studies, *J. Iran. Chem. Soc.*, 14 (2017) 1643–1649.
- [29] S. Mousavi-Mortazavi, A. Nezamzadeh-Ejhih, Supported iron oxide onto an Iranian clinoptilolite as a heterogeneous catalyst for photodegradation of furfural in a wastewater sample, *Desal. Wat. Treat.*, 57 (2016) 10802–10814.
- [30] B. Divband, A. Jodaie, M. Khatmian, Enhancement of photocatalytic degradation of 4-nitrophenol by integrating Ag nanoparticles with ZnO/HZSM-5 nanocomposite, *Iran. J. Catal.*, 9 (2019) 63–70.
- [31] R.L. Anderson, *Practical Statistics for Analytical Chemists*, Van Nostrand Reinhold, New York, 1987.
- [32] B. Rao, B. Kumar, V. Reddy, T. Rao, Preparation and characterization of CdS nano-particles by chemical co-precipitation technique, *Chalcogenide Lett.*, 8 (2011) 177–185.
- [33] N. Soltani, E. Saion, M. Hussein, M. Erfani, A. Abedini, G. Bahmanrokh, M. Navasery, P. Vaziri, Visible Light-Induced Degradation of Methylene Blue in the Presence of Photocatalytic ZnS and CdS Nanoparticles, *Int. J. Mol. Sci.*, 13 (2012) 12242–12258.
- [34] S. Songara, V. Gupta, M. Patra, J. Singh, L. Saini, G. Gowd, S. Vadera, N. Kumar, Tuning of crystal phase structure in hydrated WO<sub>3</sub> nanoparticles under wet chemical conditions and studies on their photochromic properties, *J. Phys. Chem. Solids*, 73 (2012) 851–857.
- [35] Q. -Z. Zhai, P. Wang, Preparation, characterization and optical properties of lanthanum-(nanometer MCM-41) composite material, *J. Iran. Chem. Soc.*, 5 (2008) 268–273.

- [36] H.R. Pouretdal, M. Kiyani, Photodegradation of 2-nitrophenol catalyzed by CoO, CoS and CoO/CoS nanoparticles, *J. Iran. Chem. Soc.*, 11 (2014) 271–277.
- [37] P. Dumrongrojthanath, A. Phuruangrat, S. Thongtem, T. Thongtem, Hydrothermal synthesis and characterization of visible light-driven I-doped Bi<sub>2</sub>MoO<sub>6</sub> photocatalyst, *J. Iran. Chem. Soc.*, 16 (2019) 733–739.
- [38] M. Chang, H. Zou, Y. Song, J. Chen, L. Cui, Y. Sheng, K. Zheng, Photoluminescence and photodegradation properties of SiO<sub>2</sub>@TiO<sub>2</sub>:Sm<sup>3+</sup> with different coating effects, *J. Phys. Chem. Solids*, 124 (2019) 100–110.
- [39] S. Dianat, Visible light induced photocatalytic degradation of direct red 23 and direct brown 166 by InVO<sub>4</sub>-TiO<sub>2</sub> nanocomposite, *Iran. J. Catal.*, 8 (2018) 121–132.
- [40] A. Eslami, A. Oghazyan, M. Sarafraz, Magnetically separable MgFe<sub>2</sub>O<sub>4</sub> nanoparticle for efficient catalytic ozonation of organic pollutants, *Iran. J. Catal.*, 8 (2018) 95–102.
- [41] S. Maleki, T. Madrakian, A. Afkhami, Magnetic solid-phase extraction of codeine in a biological sample utilizing Fe<sub>3</sub>O<sub>4</sub>/CDs/Lys nanocomposite as an efficient adsorbent, *J. Iran. Chem. Soc.* (2019). <https://doi.org/10.1007/s13738-019-01680-9>.
- [42] Sh. Ghattavi, A. Nezamzadeh-Ejhieh, A brief study on the boosted photocatalytic activity of AgI/WO<sub>3</sub>/ZnO in the degradation of Methylene Blue under visible light irradiation, *Desal. Wat. Treat.*, doi:10.5004/dwt.2019.24638.
- [43] R. Jiang, H.-Y. Zhu, J.-B. Li, F.-Q. Fu, J. Yao, X.-X. Liang, R.-Q. Guo, G.-M. Zeng, Efficient solar photocatalyst based on Ag<sub>3</sub>PO<sub>4</sub>/graphene nanosheets composite for photocatalytic decolorization of dye pollutants, *J. Iran. Chem. Soc.*, 13 (2016) 1167–1174.
- [44] S. Sangjan, Kh. Wisasa, N. Deddeaw, Enhanced photodegradation of reactive blue dye using Ga and Gd as catalyst in reduced graphene oxide-based TiO<sub>2</sub> composites, *Mater. Today: Proceed.*, 6 (2019) 19–23.
- [45] P. Mohammadyari, A. Nezamzadeh-Ejhieh, Supporting of mixed ZnS–NiS semiconductors onto clinoptilolite nano-particles to improve its activity in photodegradation of 2-nitrotoluene, *RSC Adv.*, 5 (2015) 75300–75310.
- [46] I. Matsuura, M. Imaizumi, M. Sugiyama, Method of kinetic analysis of photodegradation: nifedipine in solutions, *Chem. Pharm. Bull.*, 38 (1990) 1692–1696.
- [47] Ch. Lu, X. Yin, X. Liu, M. Wang, Study of the photodegradation kinetics and pathways of hexaflumuron in liquid media, *Photochem. Photobiol.*, 90 (2014) 1219–1223.
- [48] N. Omrani, A. Nezamzadeh-Ejhieh, M. Alizadeh, Brief study on the kinetic aspect of photodegradation of sulfasalazine aqueous solution by cuprous oxide/cadmium sulfide nanoparticles, *Desal. Wat. Treat.*, 162 (2019) 290–302.
- [49] J. Saïen, A.R. Soleymani, Comparative investigations on nano and micro titania photocatalysts in degradation and mineralization: use of turbidity in kinetic studies, *J. Iran. Chem. Soc.*, 6 (2009) 602–611.
- [50] M.J. Madhura, V. Gayathri, Polymer anchored copper complex as an effective catalyst for photodegradation of organic dyes, *J. Photochem. Photobiol., A*, 376 (2019) 269–278.
- [51] M. Saraji, A. Bidgoli, B. Farajmand, Hollow fiber-based liquid-liquid microextraction followed by flow injection analysis using column-less HPLC for the determination of phenazopyridine in plasma and urine, *J. Sep. Sci.*, 34 (2011) 1708–1715.
- [52] M.H. Sheikh-Mohseni, A. Nezamzadeh-Ejhieh, Modification of carbon paste electrode with Ni-clinoptilolite nanoparticles for electrocatalytic oxidation of methanol, *Electrochim. Acta*, 147 (2014) 572–581.
- [53] K.-jun Li, Q.-hua Chen, Zh. Zhang, P. Zhou, P. Li, J. Liu, J. Zhu, Determination of phenazopyridine in human plasma by GC-MS and its pharmacokinetics, *J. Chromatogr. Sci.*, 46 (2008) 686–689.

## Supplementary Data:

Table S1

Results used in Scherrer equation in the estimation of the crystallite size of CdS-WO<sub>3</sub> composite

2θ	FWHM (2θ)	β	cosθ	β cosθ	d (nm)	Av. d (nm)
16.64	0.49	0.008	0.99	0.008	17.3	22.4 ± 10.3
25.83	0.29	0.005	0.99	0.005	34.6	
30.64	0.59	0.01	0.99	0.01	15.4	
33.65	0.29	0.005	0.99	0.005	34.6	
34.40	0.19	0.003	0.99	0.003	46.2	
35.11	0.44	0.007	0.99	0.007	19.8	
38.37	0.39	0.006	0.99	0.006	23.1	
38.92	0.39	0.006	0.99	0.006	23.1	
42.99	0.78	0.01	0.99	0.01	13.8	
46.21	0.78	0.01	0.99	0.01	13.8	
49.82	0.29	0.005	0.99	0.005	27.7	
52.88	0.19	0.003	0.99	0.003	46.2	
56.43	0.34	0.006	0.99	0.006	27.7	
57.34	0.39	0.006	0.99	0.006	23.1	
61.63	0.78	0.01	0.99	0.01	13.8	
62.96	0.78	0.01	0.99	0.01	13.8	
66.25	0.78	0.01	0.99	0.01	13.8	
72.40	0.59	0.01	0.99	0.01	13.8	
74.18	0.98	0.01	0.99	0.01	13.8	
78.85	0.6	0.01	0.99	0.01	13.8	